Neural-based Quality Measurement of Fingerprint Images in Contactless Biometric Systems

Ruggero Donida Labati, Vincenzo Piuri, *Fellow, IEEE*, and Fabio Scotti, *Member, IEEE*

***Abstract*— Traditional fingerprint biometric systems capture the user fingerprint images by a contact-based sensor. Differently, contactless systems aim to capture the fingerprint images by an approach based on a vision system without the need of any contact of the user with the sensor. The user finger is placed in front of a special CCD-based system that captures the pattern of ridges and valleys of the fingertips. This approach is less constrained by the point of view of the user, but it requires much more capability of the system to deal with the focus of the moving target, the illumination problems and the complexity of the background in the captured image. During the acquisition procedure, the quality of each frame must be carefully evaluated in order to extract only the correct frames with valuable biometric information from the sequence. In this paper, we present a neural-based approach for the quality estimation of the contactless fingertips images. The application of the neural classification models allowed for a relevant reduction of the computational complexity permitting the application in real-time. Experimental results show that the proposed method has an adequate accuracy, and it can capture fingerprints at a distance up to 0.2 meters.**

I. Introduction

Contactless fingerprint biometric systems (CFBS) capture the singular pattern of ridges and valleys of the user fingertips by a CCD-based vision system. Differently from contact-based dedicated sensors, a contactless system based on a CCD camera can work in a less constrained manner since the user only need to position the fingertips in front of optics. As a main drawback, the captured images are not ready to be directly processed by a classical biometric fingerprint system, but it is needed a complex sequence of processing steps to allow the extraction of salient biometric information from the input image.

The possibility to adopt fingerprint biometric system with less constrained procedures and with no contact-based dedicated sensor has a great value since it allows for the deployment of the biometric technologies in a wider range of applications, especially in the emerging applicative field of the biometric privacy protection of user personal and sensible information [1, 2].

The goal of a CFBS is to capture and process the ridge pattern composed by the shades and the color changes on the fingertip surface in order to reconstruct the real fingerprint. Unfortunately, this task is very complex. The images captured with CFBS are very different from the images captured via contact-based dedicated sensors. The camera-based systems tend to acquire images with a poor contrast in the fingertip area and with a complex image background, while the dedicated sensors typically produce fingerprint images with high contrast and superimposed on flat and well separable backgrounds. More in detail, the background in the CFBS images is composed by two main components: the image of the surrounding environment captured around the fingertip region, and the finger itself. Notably, a large portion of the finger image can be considered as background since the real biometric information is only related to the ridge structures lying on the surface of the fingertip, and not to the colors and the fingerprint itself (Fig. 1). In addition, the presence of strong reflections on the skin due to the illumination/environmental light is capable to hide the real fingerprint pattern.

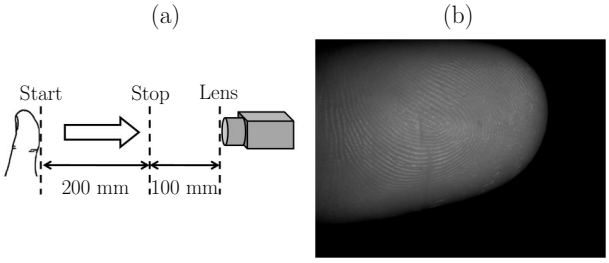

Fig. 1. A contactless fingertip system working in ambient light at high resolution: (a) the acquisition system; (b) a captured image. Only the ridge pattern in the fingertip region contains valuable biometric information. Reflections, and blurred region can occur in every frame. The proposed system can capture fingerprints at a distance up to 0.2 meters.

Considered as noise effects, the environmental light can produce different shades along the fingertip due to its intrinsic convex shape. Also, blurring effects can be present due to errors in the focus of the lenses and the relative movements of the subject in front of the camera. Moreover, the electronic noise of the CCD sensor used in the camera is always present and superimposed in the captured image.

Unfortunately, during one single fingertip capture, starting from hundreds available image frames, only a limited number of images have sufficient quality to be effectively used in a biometric system. That is due to the peculiar unconstrained setup and all the negative factors previously cited that are typically present in a CFBS application. The estimation of the image quality is crucial in the final accuracy and reliability of the whole biometric system.

Moreover, the quality of the images is related to the applica-

This work was supported in part by the EU within the 7FP project "PrimeLife" under grant agreement 216483 and by the MIUR (Ministero dell'Università e della Ricerca) under Grant 2007JXH7ET.

R. Donida Labati, V. Piuri, and F. Scotti, are with the Università degli Studi di Milano, Milano, MI 20122 Italy. They are now with the Department of Information Technologies, Università degli Studi di Milano, Crema, CR 26013, Italy (e-mails: ruggero.donida, vincenzo.piuri, fabio.scotti @unimi.it).

tive contests and the ability of the users. Each fingerprint recognition systems, in fact, can use different kinds of cameras, can work in different environmental conditions and can be projected for working with different illumination conditions.

This paper deals with the problem of the image quality assessment in CFBS. The contribute is twofold: we propose a general set of features specifically designed to represent the quality of the fingertip images in CFBS and a neural-based approach capable to extract from complex image sequences of fingertips the best frames to be used in the final biometric system. The proposed approach allows for a wider working distance of the biometric system with respect to the proposed approaches in the literature.

The performance of the proposed approach are compared with the results obtained by a well-known method in literature for the classification of the quality of fingerprint images captured with touch-based sensors released by the NIST. The execution of this method on our images requires an image preprocessing step.

The paper is structured as follows. Section II presents the state of the art of fingerprint quality identification, while section III presents the proposed methods for the feature extraction and the neural image classification. In Section IV, the proposed methods are applied to different applicative conditions, and the obtained results are then discussed and compared.

II. Related Works

In the literature, there are few studies focused on contactless systems [3 - 7]. Most systems require the placement of the finger on predisposed guides in order to simplify the image acquisition step [3 - 5]. Other proposed systems do not require a specific placement of the finger [6 - 8] but the input image must have an high quality level. In this case, the acquisition step is difficult for untrained users and the presence of a supervisor is necessary for evaluating the correctness of the acquired images. For example, in [6] is presented a fingerprint recognition system that can effectively work with low-cost CCD systems such as webcams and commercial compact cameras. Even in this case, the input image had been manually selected by a human operator during the acquisition procedure, considering the contrast level of the ridges in the input image. Such systems can work in a distance ranging from few millimeters to centimeters.

A correct placement of the finger is crucial for all the biometric recognition systems. Bad quality biometric acquisitions can generate false positives (an impostor is considered as a genuine) and false negatives (a genuine is considered as an impostor). An automatic quality control can discard the acquired images with bad quality, reducing the probability of error of the system. For example, in [9] the effect of the image quality on traditional fingerprint recognition systems is studied. The estimation of fingerprint image quality is also useful for implementing the fusion level of a monomodal multialgorithm fingerprint recognition environment [10].

In literature, there are many studies on methods for evaluating the quality of traditional fingerprint images. In [11], features related to the frequency domain (a ring structure of DFT magnitude and directional Gabor features) and to the spatial domain (black pixel ratio of the central area) are extracted and the quality is estimated by a statistical fusion criterion. The majority of the methods presented in the literature, in fact, are based on the evaluation of the intensity of small local regions of the images. In [12] a method estimate the quality of the fingerprint image by the evaluation of the probability density function (PDF) of the local regions of the fingerprint images. The method proposed in [13] is also based on the computation of local features. This features are obtained by applying Gabor filters with different orientations.

The FBI minutiae reader [14] binarizes the images through a composite approach based on a local threshold computed by evaluating the intensity of the profile in 8 directions, using 9×9 local areas. Also the fingerprint recognition systems proposed by NIST [15] are based on the computation of the mean intensity of small local regions for obtaining the threshold values used for the image binarization. The method in [16] is based on the computation of the orientation of the ridges by evaluating the intensity projection at different angles in 16×16 regions.

At the best of our knowledge, there are not available in the literature any specific studies on the quality of CFBS images.

III. The Proposed Method

The CFS images can contain four main sources of non-ideality:

- the finger is too far from the capture system and the resulting ridge pattern is not clear or sufficiently detailed;
- the finger is too close to the capture system and the obtained image is blurred since the finger is out the focus range;
- the finger is placed in skewed position with respect to the field of view of the capture system, hence and the most important characteristics of the fingerprint are not visible;
- the finger is moving too fast with respect to the exposure time of the CCD, hence motion-blurred images are produced.

The goal of the proposed method is to process in real time each frame from the capture system (Fig. 1) and to produce in output a reliable estimation of the frame quality, hence permitting to the complete biometric system to select the best frame/frames from the input sequence. The quality of fingerprint images can be expressed with continuous values (e.g., ranging from 0 to 1) or with a set of discrete values that represent classes of quality. The latter approach has been proposed by the NIST [17] and encompasses 5 level of quality, from poor to excellent. In this work we adopt a similar approach by considering an integer classification of the quality.

The methods that we propose in this paper are outlined in Fig. 2. The input image is processed by a method based on the local variance of the input image for detecting the presence of the ridges in a Region of Interest (ROI) of the input image. The method based on the local variance of the image divides the input image in M squared blocks $S_m(x_s, y_s)$ with fixed size. Then, the output image $I_A(x, y)$ is obtained applying for all the M blocks the following method

$$I_A(x,y)|_{x_s,y_s} = \begin{cases} S_b, & \text{if var}(S(x_s,y_s) \leq t1), \\ 0, & \text{otherwise.} \end{cases} \quad (1)$$

where t_1 is a fixed threshold value and x_s,y_s the pixel coordinates in the selected block. In the following we refer to ROI A as the binary image that describes $I_A(x,y) > 0$. As a second step, the ROI A is regularizated by the *flood-fill* and *open* morphological operators obtaining the binary image $I_M(x,y)$. The image $I_B(x,y)$ is computed by applying

$$I_B(x,y) = I_M(x,y) > 0 \quad (2)$$

The ROI B is equal to I_M. Fig. 2 shows in the third subplot an example of the effect of this operator. Once the filled ROI is available, we propose two different approaches. The first approach (Fig. 2, Method A) extracts from the ROI a set of features that are processed by a trained neural classifier in order to estimate the quality of the input frame.
As further discussed in the experimental result section, a direct application of the NFIQ NIST algorithm [14] to the contact-less images in not effective. Hence, we proposed a second approach (Method B in Fig. 2) capable to exploit a specific band-pass filter in order to modify that modifies the gray level intensities of the frame in order to be more similar to the patter present in a contact-based sensor. As a consequence, it is possible to adopt the NFIQ to classify the quality of the input frame. In the result section we compare and discuss the two different approach.

A. Method A

Method A is based on the extraction of a set of features from the input frames in the extracted ROI, and the subsequent classification performed by a neural classification system. As a first step, we computed 45 different features for each frame, then we applied a feature selection scheme in order to estimate the best subset of features that maximize the classification accuracy. We report a short description of the initial feature vector $F()$:

- $F(1)$:area of the ROI A;
- $F(2)$:area of the ROI B;
- $F(3)$: $F(1)/F(2)$;
- $F(4)$: standard deviation of $I_A(x,y)$;
- $F(5)$: standard deviation of $I_B(x,y)$;
- $F(6)$: standard deviation of gradient phase of $I_A(x,y)$;
- $F(7)$: standard deviation of gradient module of $I_A(x,y)$;
- $F(8)$: standard deviation of gradient phase of $I_B(x,y)$;
- $F(9)$: standard deviation of gradient module of $I_B(x,y)$;

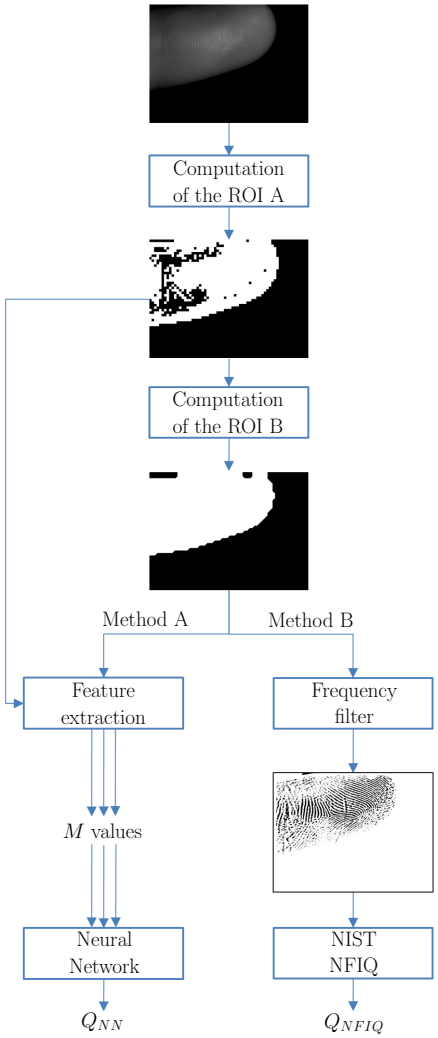

Fig. 2. Scheme of the proposed methods: the left branch of the scheme describes the Method A, the right branch of the scheme describes the Method B.

- $F(10)$-$F(11)$: coefficients of the first order polynomial that approximates the focus function $f_f()$. The focus function $f_f()$ estimate the focus level by observing the local gray-level gradient on set of candidate points placed on the edges or the ridge points in the ROI B as follow:
  - the gradient module $G_M(x,y)$ and the gradient phase $G_P(x,y)$ of $I_B(x,y)$ are computed;
  - the histogram H_{GM} of G_M is computed;
  - the cumulative frequency f_{cum} of H_{GM} is obtained by the formula

$$f(j) = H_{GM}(j) / \left(\sum_{i=0}^{255} H_{GM}(i) \right), \quad (3)$$

$$f_{cum} = \sum_{j=0}^{i} f(j); \quad (4)$$

  - the threshold intensity t is computed as

$$t = \underset{0 \leq i \leq 255}{\operatorname{argmax}} \left(f_{cum} \left(i \right) \right); \quad (5)$$

  - the set of candidate points $C_M \left(x, y \right)$ is created as

$$C_M \left(x, y \right) = G_M \left(x, y \right) \geq t; \quad (6)$$

  - a random subset $R_{CM} \left(x, y \right)$ of the set $C_M \left(x, y \right)$ is computed;
  - for each point $\left(x, y \right)$ of $R_{CM} \left(x, y \right)$ a segment $s \left(i \right)$ is computed with center in $\left(x, y \right)$, fixed length and angle normal to the value of the coordinates $\left(x, y \right)$ in $G_P \left(x, y \right)$;
  - the histogram $H_s \left(j \right)$ of the intensity of the segments $s \left(i \right)$ in the image $G_M \left(x, y \right)$ is computed;
  - the focus function $f_f \left(\right)$ is estimated as

$$f_f \left(\right) = \sum_{j=0}^{255} f \left(H \left(j \right) \right); \quad (7)$$

- $F \left(12 \right)$-$F \left(14 \right)$: coefficients of the second order polynomial that approximates the focus function $f_f \left(\right)$. The function $f_f \left(\right)$ is computed in equal fashion to computation of the features $F \left(10 \right)$ and $F \left(11 \right)$;
- $F \left(15 \right)$-$F \left(24 \right)$: values obtained computing the Fourier Discrete Transform of $I_A \left(x, y \right)$. The computation of the Fourier feature can be divided in the sequent steps:
  - all the rows of $I_A \left(x, y \right)$ are concatenated in order to produce a the linear vector $V_C \left(i \right)$;
  - the discrete Fourier transformation $V_F \left(j \right)$ of $V_C \left(i \right)$ is computed;
  - the vector $V_S \left(j \right)$ is computed by shifting the zero-frequency component of $V_F \left(j \right)$ in the central position of the vector. The number of elements in $V_F \left(j \right)$ is called N_F;
  -

$$\text{Fourier feature} = \sum_{j=N_F-N}^{N_F-1} \left| V_S \left(j+1 \right) - V_S \left(j \right) \right| \quad (8)$$

    where N is the number of the considered frequencies.

  The features are computed using N equal to $[50, 100, 150, 200, 250, 300, 350, 400, 450, 500]$ respectively.
- $F \left(25 \right)$-$F \left(34 \right)$: values obtained computing the Fourier feature of $I_B \left(x, y \right)$, using N equal to $[50, 100, 150, 200, 250, 300, 350, 400, 450, 500]$ respectively. The Fourier feature is computed in equal fashion to computation of the features from $F \left(15 \right)$ to $F \left(24 \right)$;
- $F \left(35 \right)$ normalized gray level differences in image $I \left(x, y \right)$, computed as follows

$$\Delta = \left(\max \left(I \right) - \min \left(I \right) \right) / \left(\max \left(I \right) + \min \left(I \right) \right); \quad (9)$$

- $F \left(36 \right)$: modulation of the $I_B \left(x, y \right)$;
- $F \left(37 \right)$: Signal to Noise Ratio (SNR) of $I_A \left(x, y \right)$ computed as μ / σ, where μ and σ are the mean and the standard deviation of the image;
- $F \left(38 \right)$: SNR of $I_B \left(x, y \right)$;
- $F \left(39 \right)$: Gabor feature of the $I_A \left(x, y \right)$. Gabor filters with different angles can enhance the ridges that have similar angulations in the fingerprint images. When the ridges are not sufficiently visible, the response of the Gabor filters in the output image is lower. The Gabor feature is computed as the mean of the standard deviation of the images obtained applying 8 different Gabor filters (with angles $[0, \pi/8, 1/4?, 3/8\pi, 1/2\pi, 5/8\pi, 3/2\pi, 7/8\pi]$) to the ROI.
- $F \left(40 \right)$: Gabor feature of $I_B \left(x, y \right)$. The Gabor feature is computed in equal fashion to computation of the feature $F \left(39 \right)$;
- $F \left(41 \right)$: mean of the local entropy of $I_A \left(x, y \right)$. For each pixel of an image $I \left(x, y \right)$ is computed the entropy in a 9×9 neighborhood, obtaining the local entropy image $L_E \left(x, y \right)$. The local entropy is computed starting by the histogram $H_{(x,y)} \left(i \right)$ of the local area centered in $\left(x, y \right)$ as

$$L_E \left(x, y \right) = - \sum_{i=0}^{255} H_{(x,y)} \times \log_2 \left(H_{(x,y)} \left(i \right) \right); \quad (10)$$

- $F \left(42 \right)$: mean of the local entropy $L_E \left(x, y \right)$ of $I_B \left(x, y \right)$;
- $F \left(43 \right)$: standard deviation the local entropy $L_E \left(x, y \right)$ of $I_A \left(x, y \right)$;
- $F \left(44 \right)$: standard deviation the local entropy $L_E \left(x, y \right)$ of $I_B \left(x, y \right)$;
- $F \left(45 \right)$: global entropy of the normalized image $I_{norm} \left(x, y \right)$ obtained by remapping the intinsity values of $I_{norm} \left(x, y \right)$ from 0 to 1.

The feature extraction step of the presented work aims to show different parameters that can be used to estimate the focus in the image. Depending on the available data/setup, different subsets of the proposed parameters will produce the best performance of the system in term of accuracy and computational complexity.

As a second step, we discuss the methods to automatically search for the best subset of features with respect to the available data. In this paper we considered the approach based on the wrappers algorithms [18 - 19]. We applied both classical greedy feature selection algorithm like Sequential Forward Selection, Sequential Backward Selection and a custom wrappers presented in [20], showing that remarkable improvements in the accuracy and the reduction of the complexity of the feature set are possible. Further details will be given in the experimental section.

The exact relationship between the extracted features and the frame quality is not well known, hence it is not possible to directly produce an algorithm for a classification system. The capability of the neural classifiers to learn complex input-output relationships from examples can be here exploited to create an estimation of the frame quality. In this study,

we considered feed-forward artificial neural networks to estimate frame quality in comparison with some classical classification systems such as the k-Nearest-Neighbor (kNN) classifiers and linear/quadratic discriminant classifiers. Further details will be given in the experimental section.

B. Method B

This method aims to produce a "touch equivalent" image $E(x,y)$ starting from the input frame $I(x,y)$ and then it evaluates the quality of the original transformed image by executing the NIST NFIQ algorithm [14]. The output image $E(x,y)$ is obtained by inverse Fourier transform of the product of the transformed image I and the frequency mask $M(u,v)$ as follows

$$E = \mathscr{F}^{-1}\left(\mathscr{F}\left(I_A(x,y)\cdot M\right)\right). \tag{11}$$

The mask $M(u,v)$ is computed as

$$M(u,v) = \exp\left\{\left(u^2+v^2\right)/r\right\} - \exp\left\{\left(u^2+v^2\right)/\alpha r\right\}, \tag{12}$$

where u and v are the x and y image spatial frequencies in the frequency spectrum, the parameter r is set according to the mean spatial frequency of the ridges in the images, and the parameter α is the spatial frequency bandwidth of the filter.
The final estimation of the frame quality is then given by applying the NIST NFIQ algorithm on the transformed image $E(x,y)$ as follows

$$Q_{NFIQ} = \text{NIST NFIQ}\left(E(x,y)\right) \tag{13}$$

The filter in (11), (12) produces images where only spatial wavelength related to the ridge pattern are enhanced (Fig. 2, right branch). Such filtered images are compatible with the classical approach used to estimate the fingerprint quality. We adopted the NFIQ method since it is a standard reference algorithm in the literature. This software returns five integer different quality classes.

IV. Experimental Results

A. Creation of the training and test datasets

At the best of our knowledge, there are not available any public datasets collecting touch-less fingerprint images acquired in unconstrained conditions. For this reason, we created four different dataset to test the proposed method in different operative conditions. The first dataset (Dataset A) is composed by 79 grayscale sequences with different fingers, captured with a Sony XCD-V90 camera. The frame rate is 30 fps, the size of each frame is 1920×1024 pixels, the duration of each sequence is 6s, the illumination is controlled by a led and the used focal is 25mm. For each sequences, an user brings a finger near to the camera. The range of the movement is 20mm. Each frame of the dataset had been evaluated by an experienced supervisor and labeled with its qualitative estimation in five different categories:

- Q = 5 (Poor): the ridges are not visible or the ROI is not present in the frame;
- Q = 4 (Fair): the visibility of the ridges is bad because the frame is blurred;
- Q = 3 (Good): the ridges are visible but some regions of the ROI are blurred;
- Q = 2 (Very good): the ridges are well visible;
- Q = 1 (Excellent): the ridges are clearly marked.

This task is not simple due to fact that the defocusing effect is not linear with the finger distance to the optics, and because the speed and the direction of the finger movements are not constants.
We produced other three datasets by sub-sampling the Dataset A: the first (Dataset B) is composed by 5 acquistions of the same individual (993 frames), and the second (Dataset C) is composed by 5 frame sequences related to 5 different individuals (997 frames). The Dataset D is composed by 360 random frames captured with all operative condition. Each dataset has been created in a version with 5 quality levels and in a version with two quality level (Good: quality level ≤ 1; Bad: quality level > 1). The rationale behind the two-classes datasets is to produce a simplified classifier capable to directly identify the correct frames in the sequences. In the following we refer to these dataset with the names B-5, B-2, C-5, C-2, D-5 and D-2, respectively.

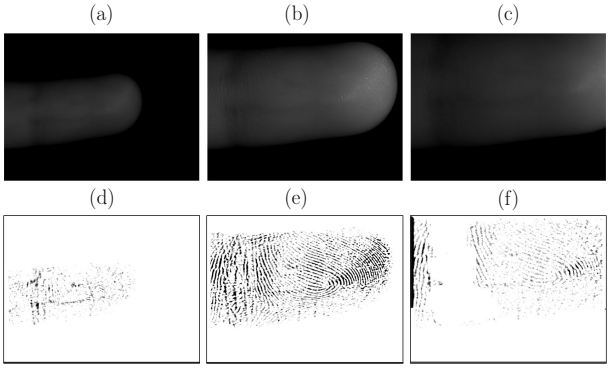

Fig. 3. Method B: Frame prefiltering. Subplots (a), (b) and (c) show examples of frames with different quality levels, while subplots (d), (e) and (f) show the output of the filter in the ROI region. The proposed filtering algorithm tends to enhance only the ridges portion in focus and it produces random-like patterns in the blurred regions. This behavior helps the subsequent NFIQ algorithm to properly estimate the quality of the frame.

B. Application of the proposed Method B

The results achievable with the proposed Method B are strictly related to the quality of the input images and to the capability of the filter (11) (12) to enhance only the ridge pattern in the image and to minimize all remaining image components. Using the proposed setup (Fig. 1) we qualitatively tuned the α filter parameter to a value equal to 10 and r equal to the height in pixel of the frame. Examples of the results of the proposed filter method are plotted in Fig. 3, where three frames with different quality are shown. The proposed filtering algorithm tends to enhance only the ridges portion in focus and it produces random-like patterns in the blurred regions. This behavior helps the subsequent

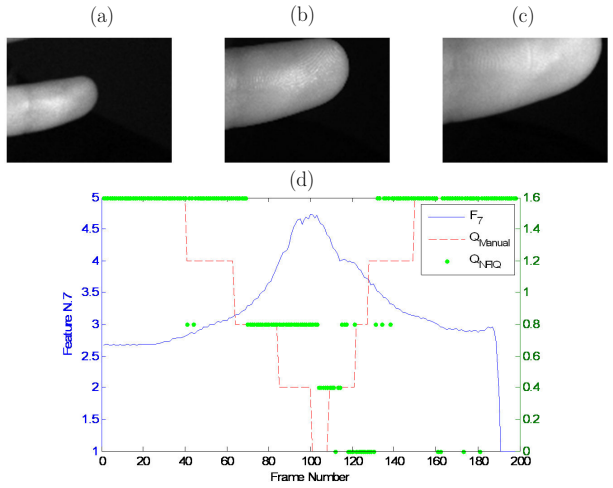

Fig. 4. Examples of the frame quality of a frame sequence. In (a), (b) and (c) are shown a poor, a good and an excellent frame, respectively; in (d) are plotted, for a complete input sequence, the quality level selected by the supervisor (dashed line), the pattern of the feature F7 of Method A (continuous line) and the quality levels produced by Method B (dotted line).

algorithms to properly estimate the quality of the frame.
As a preliminary step, in this work considered the application of the five-level approach proposed by the NIST in contactless fingerprints images. Fig. 4 plots three examples of different quality frames extracted from one sequence of Dataset A. Subplots (a), (b) and (c) show one far images, a good quality image and a out of focus image respectively. The subplot (d) shows the output of the NFIQ algorithm applied in Method B (dots) compared with supervisor evaluation (dashed line) and the output of the processed Feature 7 in the proposed Method A.

The experiments show that Method B is less robust to estimate the frame with the highest available quality estimated by the supervisor. Notably, the proposed feature $F(7)$ shows a smooth pattern and it properly follows the real image quality during the sequence. This behavior is present in all acquired sequences. The complete report of experimental results of Method B is discussed in the last subsection of the paragraph.

C. Application of the proposed Method A

In this work, we adopted the following parameters' configuration for Method A: the size of the squares $S_m(x_s, y_s)$ in (1) is 20×20 pixel, the threshold value t_1 in (1) is 0.05 and the erosion structuring element S in (2) is fixed to a squared 30×30 matrix. These parameters was tuned by empirical tests on the available images.
After the parameters setting step, the proposed method encompasses the features selection step. The produced main Dataset A has 14220 frames, hence it is almost impossible to manage such quantity of features vectors with the best wrapper algorithms available in the literature (subsection III-A). For this reason we used three different subsampled dataset that containing different operative condition of the setup. Experiments showed that the most effective feature selection method for our dataset is the *forward selection technique* [21]. The feature selection phase produced the estimated best features set for each of the dataset B-5, B-2, C-5, C-2, D-5 and D-2. Further details are available in the next subsection.
In our experiments we tested different classification paradigms in order to better study the complexity of the learning problem embedded in the six datasets. In particular, we adopted the following classifier families:

- the Linear Bayes Normal Classifier (LDC);
- the Quadratic Bayes Normal Classifier (QDC);
- the k-Nearest Neighbor classifier with odd values of the parameter $k\,(1, 3, 5)$;
- feed forward neural networks with different number of neurons in the hidden layer.

In order to effectively estimate the generalization error of the trained neural networks, we adopted a simple N-fold cross validation technique with $N = 10$ [22]. The topology of the neural networks has been designed as follows: we used a linear node as output layer for the neural networks and we tested different number of nodes in the hidden layer. The selected topology for the nodes of this layer is log-sigmoidal. The algorithm used for train the neural networks is the back-propagation algorithm.

D. Final results and discussion

Table I reports the best subsets of features related to the six datasets obtained by the forward selection technique. Table II resumes the obtained results of the neural-based classification system compared with the classical inductive classification methods for all datasets, and with respect to the performance of Method B. In particular, Table II reports only the best configuration found during the analysis (Number of hidden layer for the neural networks, the k-parameter for the kNN classifier and the best feature sets selected by the Sequential Forward Selection algorithm).
Table II shows that Method A offers a remarkable accuracy compared with Method B in all datasets. In addition, the neural-based classifier shows a very good accuracy compared with other classical inductive classification system. The only classification family showing a similar accuracy (on the considered datasets) are the kNN classifiers, but the neural network approach offers a relevant gain in the computational complexity. Table III shows the computational gain of the neural networks compared by kNN classifier. This gain depends on the number of sample stored in the k-NN classifier, compared to the number of neurons in the neural networks. Considering the datasets B-5, B-2, C-5, C-2, D-5 and D-2, the minimum gain factor found is equal to 36. Experiments showed that the Method A applied with the neural-based quality classification system is the most suitable for the real-time applications.

All presented methods have been written in Matlab language (Version 7.6) exploiting the available toolboxes on Intel Centrino 2.0Ghz working with Windows XP.

TABLE II

FEATURE SUBSETS

Dataset	Method A								Method B
	Linear		NN-3		NN-5		kNN		
	mean	std	mean	std	mean	std	mean	std	mean
B-5	0.191	0.002	0.046	0.004	0.065	0.004	0.042	0.004	0.478
B-2	0.083	0.000	0.013	0.000	0.017	0.004	0.011	0.001	0.140
C-5	0.239	0.004	0.066	0.008	0.065	0.001	0.068	0.000	0.358
C-2	0.049	0.001	0.013	0.002	0.016	0.001	0.015	0.003	0.150
D-5	0.354	0.006	0.275	0.008	0.286	0.012	0.278	0.016	0.469
D-2	0.047	0.000	0.064	0.024	0.047	0.000	0.050	0.000	0.180

Notes. Classification methods of Method A: Linear Classifier (Linear); Feed-Foreword Neural Network with one hidden layer composed by 3 nodes (NN-3); Feed-Foreword Neural Network with one hidden layer composed by 5 nodes (NN-5); kNN with k=1 (kNN). The datasets B-5, C-5 and D-5 are classified in five different classes. The datasets B-2, C-2 and D-2 are classified in two different classes.

TABLE I

FEATURE SUBSETS

Dataset	Feature Subset
B-5	[1, 2, 6, 7, 35, 40, 41, 45]
B-2	[1, 3, 6, 7, 8, 31, 37, 38, 42]
C-5	[1, 6, 7, 41, 42, 43, 45]
C-2	[2, 3, 6, 7, 29, 31, 36, 45]
D-5	[6, 8, 35, 45]
D-2	[4, 6, 10, 11, 12, 13, 16, 27, 33, 44]

Notes. The datasets B-5, C-5 and D-5 are classified in five different classes. The datasets B-2, C-2 and D-2 are classified in two different classes.

The computational time of the Method A is different for each dataset/classifier.

TABLE III

COMPUTATIONAL GAIN

Dataset	Computational Gain
B-5	201.459
B-2	205.527
C-5	121.756
C-2	539.839
D-5	159.852
D-2	46.456

The computational gain is processed by the ratio of the computational time required by the most accurate traditional classifier to the computational time of the most accurate neural network. Accuracy are reported in Table II.

The total computational time is also related to the feature extraction. The computation of the majority of the features requires less than 0.05 s. The features $F(39)$ and $F(40)$ require about 2.3 s and the feature $F(41)$, $F(42)$, $F(43)$ and $F(44)$ require about 4 s. The features $F(10)$ and $F(11)$ are computed at the same time and this step requires about 1.2 s. In a similar fashion, the computation of the features $F(12)$, $F(13)$ and $F(14)$ requires about 1.2 s. The feature selection step showed that these computational-heavy features are not strictly needed to guarantee the best accuracy of the system, and they can be replaced by subsets of relatively simple features.

The bottleneck of the Method A consists in the estimation of the ROIs. Implementation of the ROI A and ROI B that are not suitably optimized can require up to 1.5s and 3.7s, respectively. On the contrary, optimized versions reduced the computational complexity by two orders of magnitude solving this crucial issue to achieve the real-time goal.

V. CONCLUSIONS

This paper presented an approach for the quality measurement of contactless fingerprint images based on a neural classification system. Classical quality assessment systems present in the literature designed for contact-based fingerprint sensors are not adequate for contactless fingerprint images. The paper presented an alternative set of features capable to deal with the contactless setups and it describes the designing and training and the final neural classification system. Experimental results show that the presented method is achievable and it offers suitable accuracy in a working distance range up to of 0.2 m. Further studies will be focused on the optimization of the computational complexity of the method as well as on the study of effect of different environmental conditions.

REFERENCES

[1] S. Cimato, M. Gamassi, V. Piuri, R. Sassi, and F. Scotti, "Privacy in biometrics," in *Biometrics: Theory, Methods, and Applications*. Wiley-IEEE Press, 2008, 978-0-470-24782-2.

[2] S. Cimato, M. Gamassi, V. Piuri, R. Sassi, and F. Scotti, "Privacy-aware biometrics: Design and implementation of a multimodal verification system," in *ACSAC*, 2008, pp. 130–139.

[3] G. Parziale, E. Diaz Santana, and R. Hauke, "The surround imagertm: A multi-camera touchless device to acquire 3d rolled-equivalent fingerprints," 2006, pp. 244–250.

[4] Y. Wang, L. Hassebrook, and D. Lau, "Noncontact, depth-detailed 3d fingerprinting," vol. Newsroom, 2009.

[5] S. Mil'shtein, J. Palma, C. Liessner, M. Baier, A. Pillai, and A. Shendye, "Line scanner for biometric applications," may 2008, pp. 205 –208.

[6] V. Piuri and F. Scotti, "Fingerprint biometrics via low-cost sensors and webcams," 29 2008-oct. 1 2008, pp. 1 –6.

[7] B. Hiew, A. Teoh, and Y. Pang, "Touch-less fingerprint recognition system," june 2007, pp. 24 –29.

[8] B. Y. Hiew, A. B. J. Teoh, and D. C. L. Ngo, "Automatic digital camera based fingerprint image preprocessing," in *CGIV '06: Proceedings of the International Conference on Computer Graphics, Imaging and Visualisation*. Washington, DC, USA: IEEE Computer Society, 2006, pp. 182–189.

[9] J. Fierrez-Aguilar, L. Munoz-Serrano, F. Alonso-Fernandez, and J. Ortega-Garcia, "On the effects of image quality degradation on minutiae- and ridge-based automatic fingerprint recognition," oct. 2005, pp. 79 – 82.

[10] Y. Chen, S. Dass, and A. Jain, "Fingerprint quality indices for predicting authentication performance," in *In: Proc. AVBPA, Springer LNCS-3546*, 2005, pp. 160–170.

[11] D. Yu, L. Ma, H. Lu, and Z. Chen, "Fusion method of fingerprint quality evaluation: From the local gabor feature to the global spatial-frequency structures," 2006, pp. 776–785.
[12] S. Lee, H. seung Choi, K. Choi, and J. Kim, "Fingerprint-quality index using gradient components," *IEEE Transactions on Information Forensics and Security*, vol. 3, no. 4, pp. 792–800, 2008.
[13] L. Shen, A. C. Kot, and W. M. Koo, "Quality measures of fingerprint images," in *AVBPA*, 2001, pp. 266–271.
[14] R. Stock and C. Swonger, "Development and evaluation of a reader of fingerprint minutiae," Cornell Aeronautical Laboratory, Technical Report CAL No. XM-2478-X-1:13-17, 1969.
[15] M. Garris, E. Tabassi, and C. Wilson, "Nist fingerprint evaluations and developments," vol. 94, no. 11, pp. 1915–1926, November 2006.
[16] N. K. Ratha, S. Chen, and A. K. Jain, "Adaptive flow orientation-based feature extraction in fingerprint images," *Pattern Recognition*, vol. 28, no. 11, pp. 1657 – 1672, 1995.
[17] E. Tabassi, C. Wilson, and C. Watson, "Fingerprint image quality," National Institute of Standards and Technology (NIST), Technical Report NISTIR 7151, August 2004.
[18] R. Kohavi and G. H. John, "Wrappers for feature subset selection," *Artif. Intell.*, vol. 97, no. 1-2, pp. 273–324, 1997.
[19] I. Guyon and A. Elisseeff, "An introduction to variable and feature selection," *J. Mach. Learn. Res.*, vol. 3, pp. 1157–1182, 2003.
[20] C. Alippi, P. Braione, V. Piuri, and F. Scotti, "A methodological approach to multisensor classification for innovative laser material processing units," vol. 3, 2001, pp. 1762 –1767 vol.3.
[21] A. K. Jain, R. P. Duin, and J. Mao, "Statistical pattern recognition: A review," *IEEE Transactions on Pattern Analysis and Machine Intelligence*, vol. 22, pp. 4–37, 2000.
[22] R. O. Duda, P. E. Hart, and D. G. Stork, *Pattern Classification (2nd Edition)*, 2nd ed. Wiley-Interscience, November 2000.